The phosphatase inhibitor Sds23 regulates cell division symmetry in fission yeast

Katherine L. Schutt and James B. Moseley*

Department of Biochemistry and Cell Biology
The Geisel School of Medicine at Dartmouth, Hanover, NH 03755

* Corresponding author
james.b.moseley@dartmouth.edu

Running Title: Sds23 regulates division symmetry in fission yeast

Character count: 19,952

Abstract
Animal and fungal cells divide through the assembly, anchoring, and constriction of a contractile actomyosin ring (CAR) during cytokinesis. The timing and position of the CAR must be tightly controlled to prevent defects in cell division, but many of the underlying signaling events remain unknown. The conserved heterotrimeric protein phosphatase PP2A controls the timing of events in mitosis. Upstream pathways including Greatwall-Ensa regulate PP2A activity. A role for PP2A in CAR regulation has been less clear, although loss of PP2A in yeast causes defects in cytokinesis. Here, we report that Sds23, an inhibitor of PP2A family protein phosphatases, promotes the symmetric division of fission yeast cells through spatial control of cytokinesis. We found that *sds23*Δ cells divide asymmetrically due to misplaced CAR assembly, followed by sliding of the CAR away from its assembly site. These mutant cells exhibit delayed recruitment of putative CAR anchoring proteins including the glucan synthase Bgs1. Our observations likely reflect a broader role for regulation of PP2A in cell polarity and cytokinesis because *sds23*Δ phenotypes were exacerbated when combined with mutations in the fission yeast Ensa homolog, Igo1. These results identify the PP2A regulatory network as a critical component in the signaling pathways coordinating cytokinesis.

Introduction

Organisms from yeast to humans build a contractile actomyosin ring (CAR) that drives cytokinesis. The fission yeast CAR assembles from a series of 50-75 precursor structures termed "nodes" in the plasma membrane (Chang *et al.*, 1996; Sohrmann *et al.*, 1996; Wu *et al*., 2006; Almonacid *et al.*, 2009; Almonacid *et al.*, 2011). Similar precursors have been observed in animal cell CAR assembly (Piekny and Glotzer, 2008). Nodes contain actin- and myosin-regulatory proteins, as well as membrane-binding proteins with the capacity to tether the CAR to the cell cortex (Wu *et al.*, 2006). During mitosis, nodes coalesce into an intact CAR. Past studies have defined the recruitment timing, functional contribution, and spatial organization of CAR proteins in fission yeast (Pollard and Wu, 2010; Laplante *et al.*, 2016; McDonald *et al.*, 2017).

However, many questions remain open regarding the upstream signaling pathways that ensure assembly of this complex structure at the correct time and place.

Fission yeast cells proceed through cytokinesis in three steps. The first step is CAR formation, when precursor nodes congress to form an intact ring (Wu *et al.*, 2006). Nodes are positioned in the cell middle by positive signals from the nucleus, and by inhibitory signals from the protein kinase Pom1 at cell tips (Bähler and Pringle, 1998; Daga and Chang, 2005; Celton-Morizur *et al.*, 2006; Padte *et al*., 2006). Both signals converge on the anillin-like scaffold protein Mid1 (Celton-Morizur *et al.,* 2006; Padte *et al.,* 2006*;* Almonacid *et al.*, 2009; Almonacid *et al.*, 2011). The second step is CAR maturation, when additional proteins are recruited to the division site (Wu *et al.*, 2003; Wu *et al.*, 2006; Pollard and Wu, 2010). During maturation, the CAR must be anchored in place to prevent sliding towards cell ends. Several proteins have been implicated in anchoring the CAR. These proteins include the cell wall synthase Bgs1 (Arasada and Pollard, 2014; G. Cortés *et al.*, 2015; Sethi *et al*., 2016), the membrane-binding protein Cdc15 (Arasada and Pollard, 2014; McDonald *et al.*, 2015; Snider *et al*., 2017), regulators of the lipid PI(4,5)P_2 (Snider *et al.*, 2017; Snider *et al.*, 2018), and the scaffolding protein Pxl1 (G. Cortés *et al*., 2015). The third step is CAR constriction, which must be coordinated with septum assembly (Liu *et al.*, 1999; Sipiczki and Bozsik, 2000; Liu *et al.*, 2002). Both CAR constriction and septation contribute to the force required for cytokinesis and cell separation (Jochová *et al.*, 1991; Proctor *et al.*, 2012).

In fission yeast and other systems, protein kinases provide spatial and temporal regulation of cytokinesis. Protein phosphatases, which counter the activity of protein kinases, therefore represent potential regulators of cytokinetic events. In human cells, phosphatases have recently been linked to cytokinesis (Burgess *et al.*, 2010; Cundell *et al.*, 2013). In fission yeast, the phosphatases calcineurin and Clp1 localize to the division site and regulate the timing of cytokinetic events (Trautmann *et al.,* 2001; Mishra *et al.,* 2004; Clifford *et al.*, 2008; Martín-García *et al.*, 2018). Fission yeast mutants in the conserved heterotrimeric phosphatase PP2A have suggested a role for this phosphatase in cytokinesis, but how regulation of PP2A might connect to specific steps in cytokinesis is unclear (Kinoshita *et al.*, 1996; Jiang and Hallberg, 2001; Le Goff *et al.*, 2001; Lahoz *et al.*, 2010; Goyal and Simanis, 2012). PP2A mutants exhibit defects in diverse cellular processes, making it challenging to obtain a clear connection with cytokinesis. PP2A is itself regulated by a number of upstream factors, which might control specific aspects of PP2A function. We reasoned that mutating these regulators could provide a way to study how this conserved phosphatase regulates cytokinesis without affecting other cellular functions.

In this study, we have identified and characterized cytokinesis defects in cells lacking Sds23, which binds to and inhibits PP2A-related phosphatases (Hanyu *et al.*, 2009; Deng *et al.*, 2017). We found that the CAR assembles off-center in *sds23*Δ mutants, and once assembled slides away from the cell middle due to delayed recruitment of potential anchors. The asymmetric division phenotype of *sds23*Δ cells is exacerbated when combined with deletion of a second inhibitor of PP2A, Igo1 (Chica *et al.*, 2016), suggesting that Sds23 and Igo1 cooperate to control PP2A and are required for spatial control of cytokinesis.

Results and Discussion

Cells lacking Sds23 divide asymmetrically

While studying Sds23 in nutrient signaling (Deng *et al.*, 2017), we observed that *sds23*Δ cells divide with off-center septa (Figure 1A). We quantified this defect by measuring the Cell

Half Ratio (Figure 1B) (Snider *et al.*, 2017), which confirmed a significant defect in positioning the division plane for *sds23*Δ cells compared to wild type cells (Figure 1C). At division, *sds23*Δ cells are longer than wild type cells, so we considered the possibility that increased cell length caused the measured division asymmetry. To address this idea, we used a *cdc25-degron-DAmP* (hereafter, *cdc25-dd*) strain, which divides at a similar length to *sds23*Δ (Figure 1A). We found that *cdc25-dd* cells divide as symmetrically as wild type cells, indicating that asymmetric division of *sds23*Δ cells is not due to cell length (Figure 1C). The *sds23*Δ and *cdc25-dd* mutations had additive defects in cell length, but *sds23*Δ *cdc25-dd* double mutant cells displayed the same Cell Half Ratio as *sds23*Δ single mutants (Figure 1C). We conclude that Sds23 regulates the position of the division plane independent of cell size.

sds23 mutants fail to assemble and to anchor the CAR in the cell middle

We next investigated the cause of misplaced division planes in *sds23*Δ cells. We monitored the position and timing of CAR assembly using *rlc1-mNeonGreen* (hereafter, *rlc1-mNG*) *sad1-mEGFP* cells. Rlc1 marks the precursor nodes and CAR, and Sad1 marks the spindle pole bodies, which provide a clock for cytokinetic events (Wu *et al.*, 2003). CAR formation occurred with the same timing in *sds23*Δ and wild type cells, but was misplaced in *sds23*Δ cells (Figure 2, A and B). Misplaced ring assembly is not due to delocalized Pom1, which remained at cell tips in *sds23*Δ cells (Supplemental Figure 1A). Similarly, off-center ring formation was not caused by changes in the localization of Cdr2 nodes, which are themselves precursors to cytokinetic nodes (Supplemental Figure 1B). Thus, the off-center CAR phenotype of *sds23*Δ cells does not reflect changes to Pom1-dependent negative spatial cues.

In addition to Pom1-dependent negative spatial cues, spatial control of CAR formation also depends on positive cues from the nucleus. Using Cut11-mCherry to mark the nucleus, we performed time-lapse imaging of wild type and *sds23*Δ cells. In wild type cells, the nucleus remained stationary at the center of cells (Figure 2, C and D), consistent with normal medial placement of the CAR in these cells. In *sds23*Δ cells, the nucleus was not stationary at the cell middle, and instead wandered off-center (Figure 2, C and D). Importantly, nuclear positioning and nuclear movement in elongated *cdc25-dd* cells resembled wild type (Figure 2, C and D). Nuclear wandering could promote off-center CAR formation through mislocalization of positive spatial cues. To test this, we analyzed Mid1, which shuttles between the nucleus and precursor nodes to coordinate spatial cues from these two structures (Bähler *et al*., 1998a; Daga and Chang, 2005; Almonacid *et al*., 2009). Mid1-mNeonGreen protein levels were reduced in *sds23*Δ cells (Figure 2E) and displayed reduced levels in the nucleus (Figure 2F). Node localization of Mid1-mNeonGreen was not strongly impaired in *sds23*Δ cells (Figure 2F), but reduced levels of Mid1-mNeonGreen were recruited to the CAR (Supplemental Figure 2K). Thus, *sds23*Δ cells have defects in nuclear positioning and in Mid1 localization. These defects likely lead to misplaced CAR assembly away from the cell middle.

Once assembled, the CAR must be anchored in place during the maturation phase of cytokinesis. In certain mutants, CARs can assemble properly but then slide away from the cell middle, resulting in asymmetric division. This defect has been observed in mutants that alter plasma membrane PI(4,5)P_2 regulation (Snider *et al.*, 2017; Snider *et al*., 2018), or upon mutation of Cdc15, an essential F-BAR domain protein that might tether the CAR to the plasma membrane (Arasada and Pollard, 2014; McDonald *et al.*, 2015; Snider *et al*., 2017). To determine if ring sliding defects occur in *sds23*Δ cells, we performed time-lapse imaging on *rlc1-mNG sad1-mEGFP* cells. After ring formation, CARs in wild type or elongated *cdc25-dd* cells

did not move from their initial position (Figure 3A). In contrast, CARs in *sds23*Δ cells slid away from their initial position (Figure 3A). We measured ring displacement (Figure 3B, Top) and found that CARs slid significantly farther in *sds23*Δ cells than in wild type or *cdc25-dd* cells (Figure 3B, Bottom). In these experiments, CARs slid during the time period corresponding to ring maturation, which occurs after assembly but before constriction. We measured a significantly longer maturation phase in *sds23*Δ versus wild type cells (Figure 3C), indicating that this CAR stage requires Sds23 to proceed normally. We tested if this Sds23 function connects with PI(4,5)P_2 regulation by combining *sds23*Δ with *efr3*Δ. Efr3 is a scaffold for PI-4 kinase, and *efr3*Δ cells were recently shown to exhibit ring sliding (Snider *et al.*, 2017) (Figure 1, A and C). The *sds23*Δ *efr3*Δ double mutant cells rapidly lysed (Figure 3D), suggesting a synthetic effect that indicates that Sds23 likely promotes CAR anchoring through a different pathway from PI(4,5)P_2 regulation.

Sds23 is required for timely recruitment of CAR anchors

Reduced recruitment of proteins that anchor the CAR in place could explain both the ring sliding and extended maturation phase of *sds23*Δ mutant cells. To test this hypothesis, we measured the levels of 20 cytokinesis proteins at the CAR using live-cell microscopy of wild type or *sds23*Δ cells (Supplemental Figure 2, A-T). Several proteins that might contribute to ring anchoring were present in reduced levels at the CAR of *sds23*Δ cells. These proteins include Bgs1, a transmembrane cell wall enzyme, and Imp2 and Rga7, which both contain membrane-binding F-BAR domains (Supplemental Figure 2, A, B and P) (Demeter and Sazer, 1998; Martin-Garcia *et al.*, 2014; McDonald *et al.*, 2016). We did not detect altered levels of Cdc15, another F-BAR domain containing protein that is implicated in ring anchoring (Supplemental Figure 2C) (Roberts-Galbraith *et al.*, 2009; McDonald *et al.*, 2015).

Past work has suggested that delayed recruitment of Bgs1, which synthesizes 1,3-beta-glucan for the primary septum, can lead to ring sliding (Arasada and Pollard, 2014), potentially because the cell wall provides a static anchor for CARs. We measured the timing of GFP-Bgs1 recruitment in *sds23*Δ and wild type cells using the SPB clock (Wu *et al.*, 2003). Bgs1 recruitment to the division site was delayed 10-15 minutes in *sds23*Δ compared to wild type cells (Figure 4, A and B), consistent with a similar extension in the maturation phase of cytokinesis in this mutant. We observed similar delays in Imp2-GFP (~5 minutes) (Figure 4, C and D) and Rga7-GFP (~10-15 minutes) (Figure 4, E and F) recruitment in *sds23*Δ cells compared to wild type cells. Such delays were specific to these factors, as other proteins such as Rlc1 were recruited to the CAR with similar kinetics in *sds23*Δ and wild type cells (Supplemental Figure 1C). We conclude that Sds23 is required for the timely recruitment of specific putative CAR anchoring proteins. In *sds23*Δ cells, ring constriction does not commence until sufficient levels of key proteins including Bgs1 accumulate. This delay causes an extended maturation phase with reduced levels of CAR anchors, likely leading to ring sliding.

Genetic interactions between Sds23 and the Greatwall Kinase Pathway

Sds23 physically associates with PP2A and PP6 phosphatases, and can inhibit PP6 phosphatase activity (Hanyu *et al.*, 2009; Deng *et al.*, 2017). To determine if phosphatase regulation contributes more generally to division plane positioning, we tested the genetic interaction of *sds23*Δ with *igo1*Δ. Similar to other organisms, the fission yeast endosulfine protein Igo1 inhibits PP2A activity (Chica *et al.*, 2016). The Greatwall kinase Ppk18 phosphorylates and activates Igo1, raising the possibility that Ppk18-Igo1 and Sds23 might

provide dual regulatory arms for PP2A phosphatases (Figure 5A) (Chica *et al.*, 2016). Both *igo1*Δ and *ppk18*Δ mutants alone did not display defects in cell shape or division symmetry under normal growing conditions, consistent with previous reports (Figure 5, B-D) (Chica *et al.*, 2016). However, combining either mutation with *sds23*Δ led to synthetic defects. First, the percentage of cells with aberrant morphology, specifically bent and curved cells, was increased in the *sds23*Δ *igo1*Δ and *sds23*Δ *ppk18*Δ double mutant cells compared to single mutants (Figure 5C). Second, the double mutant cells divided more asymmetrically than *sds23*Δ single mutants (Figure 5D). This synthetic defect was not due to the longer cell phenotype of *sds23*Δ, as combining *igo1*Δ with *cdc25-dd* had no effect on division plane positioning (Supplemental Figure 3, A and B). These genetic experiments reveal a previously unknown role for the Greatwall kinase pathway in cell polarity and cytokinesis. Synthetic defects between Sds23 and Ppk18-Igo1 support a broad role for PP2A-family regulators in positioning the division plane.

Conclusions

Our results define a new role for regulation of PP2A in cytokinesis and cell division. Past work has shown that *sds23*Δ cells exhibit increased levels of PP2A activity (Hanyu *et al.*, 2009), and our results show that these cells have defects in recruiting key cytokinesis proteins such as Mid1 and Bgs1 to the division site. These recruitment defects likely underlie misplaced assembly of the CAR and its subsequent sliding away from the cell middle. Future experiments will address if these cytokinesis proteins are direct targets of dysregulated PP2A or if their dysregulation occurs farther downstream of PP2A signaling. PP2A has been proposed to counter the septation initiation network (SIN) in fission yeast (Jiang and Hallberg, 2000; Jiang and Hallberg, 2001; Le Goff *et al.*, 2001; Lahoz *et al.*, 2010), therefore, Sds23 and Igo1 action on PP2A may alter the balance of PP2A versus SIN activity within the cell, leading to the division phenotypes observed in this study.

The ability of an intact CAR to slide laterally within the plane of the plasma membrane indicates a remarkable level of structural integrity and stability, even though many components are exhibiting rapid flux as shown by photobleaching experiments (Pelham and Chang, 2002). It seems likely that the CAR is anchored in place by multiple tethers, including the components implicated in this study as well as previous work (Arasada and Pollard, 2014; McDonald *et al.*, 2015; Snider *et al.*, 2017). Such a multi-component anchoring system may facilitate a spatial control system that is robust during dynamic processes including septum synthesis, vesicle delivery, and CAR constriction.

Our work places this PP2A regulatory network in the growing context of protein phosphatases that control cytokinesis. Given the roles of PP2A in diverse cellular functions, it will be interesting to know how potential cytokinesis targets are regulated with specificity in time and space. The partially overlapping roles of Sds23 and Igo1 in this regulatory system, as shown by synthetic genetic defects, raise possibilities for dynamic control of cytokinesis by PP2A during cell cycle progression. The Greatwall-endosulfine pathway including Ppk18-Igo1 is best known for regulation of mitotic entry (Mochida *et al.*, 2010; Burgess *et al.*, 2010; Chica *et al.*, 2016), and Sds23 has also been linked to cell cycle progression through phenotypes such as cell size (Ishii *et al*., 1996; Jang *et al*., 1997; Deng *et al*., 2017). These functional connections to the cell cycle suggest that timely regulation of PP2A by these proteins could ensure proper cytokinesis. Both Sds23 and Igo1 are known to be hyperphosphorylated, which may serve to regulate their interactions with PP2A (Hanyu *et al.*, 2009; Chica *et al.*, 2016). We also note that the Ppk18-Igo1 pathway is upregulated during nitrogen stress (Chica *et al.*, 2016), and Sds23

functions in pathways upregulated during glucose depletion and energy stress (Yakura *et al.*, 2006; Hanyu *et al.*, 2009; Jang *et al.*, 2013; Saitoh *et al.*, 2015; Deng *et al.*, 2017). Thus, it will be interesting to determine how these pathways contribute to cytokinesis when cells encounter environmental stresses linked to their functions. Given the conservation of PP2A complexes and functions in yeast through humans, phosphatase regulation by proteins such as those described here might contribute to robust cytokinesis in diverse cell types and organisms.

Materials and Methods

Yeast Strains and Growth

Standard *S. pombe* media and methods were used (Moreno *et al.*, 1991). Strains used in this study are listed in Supplemental Table 1. Gene tagging and deletion were performed using PCR and homologous recombination (Bähler et al., 1998b), and integrations were verified by colony PCR, microscopy, and/or western blot. To cross the sterile mutant *sds23*Δ*,* a pJK148 plasmid with *sds23+* or *sds23-mNeonGreen+* was integrated at the *leu1* locus of a *sds23*Δ*::natR leu1-32* strain, and *leu1-32 natR* progeny or *natR* progeny lacking *mNeonGreen* signal were selected from subsequent crosses.

Microscopy

All image analysis was performed on ImageJ (National Institutes of Health) (Schneider *et al*., 2012). For Figure 1A and Supplemental Figure 3A, cells were grown at 32˚C, stained with Blankophor (MP Biomedicals), mounted on a glass slide under a coverslip, and middle focal plane images were obtained at room temperature. Imaging was performed on a Deltavision Imaging System (Applied Precision/GE Healthcare), which used a customized Olympus IX-71 inverted wide-field microscope, a Photometrics Cool-SNAP HQ2 camera, Insight solid-state Illumination unit and 1.42 NA Plan Apo 60x oil objective. For Figure 3D, cells were grown at 32˚C, mounted on a glass slide under a coverslip, and middle focal plane images were obtained at room temperature using the Deltavision Imaging System. For Supplemental Figure 1A, cells were grown at 32˚C, mounted on a glass slide under a coverslip, and middle focal plane images were acquired at room temperature using the Deltavision Imaging System. For Supplemental Figure 1B, cells were grown at 32˚C, mounted on a glass slide under a coverslip, and z-sectioning was performed with images acquired every 0.5 µm for 6 µm (12 steps). Images were acquired using the Deltavision imaging system and z-stacks were processed by iterative deconvolution in SoftWorx Software (Applied Precision/GE Healthcare). To calculate FWHM, a rectangular ROI of 160 pixels x 48 pixels was drawn around cells that were between 15-17 µm in length and fluorescence profile for Cdr2-mEGFP was plotted. A Gaussian distribution was fitted to this fluorescence profile for each cell using the Least Squares Regression method in Graphpad Prism, and FWHM was calculated by the following equation: $2*(\sqrt{(2\ln 2)})*SD$, where SD is the standard deviation. Each point represents a single cell and statistical analysis was performed by unpaired t-test with Welch's Correction. For Figure 5B, cells were grown at 32˚C, stained with Blankophor (MP Biomedicals), mounted on a glass slide under a coverslip, and middle focal plane images were obtained using a Nikon Eclipse Ti microscope equipped with an Andor Zyla camera, Perfect Focus and a Tokai Hit stage incubator maintained at 32˚C and using a Plan Apo λ 1.4 NA aperture 60x oil objective.

For Cell Half Ratio analysis, cell length of each daughter cell was measured from Blankophor stained images, and Cell Half Ratio was calculated by dividing the short half by the long half. For statistical analysis in Figure 1C, a one-way Anova with Tukey's multiple comparisons test was performed. For Figures 2C, 3A, 4A, 4C, 4E, and Supplemental Figure 1C cells were imaged at 32˚C using a Andor W1 Spinning Disk Confocal, set up on a Nikon Eclipse Ti inverted microscope stand with Perfect Focus and Tokai Hit stage incubation system using a Plan Apo λ 1.4 NA aperture 60x oil objective. For imaging, ~1 µl of cells were mounted on EMM4S agarose pads (1.4% InCert™ Agarose, Lonza) and sealed under a coverslip with VALAP (Vaseline, Lanolin, Parrafin). For Figures 2B and 3C, ring assembly and maturation timing were determined from time-lapse movies of Rlc1-mNeonGreen and Sad1-mEGFP

expressing cells that were imaged every 5 minutes. Ring assembly was determined as the time it took from SPB splitting to form an intact CR. Ring maturation was determined as the time between ring assembly and prior to constriction. Each point represents a single cell. For statistical analysis, a one-way ANOVA with Tukey's multiple comparisons was used. For Figure 2F, cells were grown at 32˚C, mounted on a glass slide under a coverslip, and maximum intensity projections were generated using 0.5-µm focal planes throughout the entire cell (13 steps, 6 µm total). Images were obtained using the Andor W1 Spinning Disk Confocal and a Tokai Hit stage incubator maintained at 32˚C and using a Plan Apo λ 1.45 NA 100x oil objective.

For images in Figure 2C, single focal plane images in the cell middle were acquired every 3 minutes. To measure nuclear movement a line was drawn from the center of the nucleus to the cell tip, and the length of this line was measured at every time point. Nuclear movement (µm/min) was quantified as the average difference between those lengths between every time point, divided by 3 minutes. Each point in Figure 2D is the average for a single cell with 10 cells measured per strain. For statistical analysis of nuclear movement, a one-way ANOVA with Tukey's multiple comparisons test was used. For images in Figure 3A, images were acquired every 5 minutes and sum intensity projections were generated using 0.5-µm focal planes throughout the entire cell (11 steps, 5 µm total). For displacement measurements in Figure 3B, the length of one cell half was measured at ring formation and the length of that same cell half was measured at final ring constriction. The difference between these two values was quantified as the ring displacement (µm) (See Figure 3B schematic). Each dot in Figure 3B corresponds to a single cell and for statistical analysis a one-way ANOVA with Tukey's multiple comparisons test was used.

For Figures 4A, 4C, 4E, and Supplemental Figure 1C images were acquired every 5 minutes using the Andor W1 Spinning Disk Confocal and sum intensity projections were generated using 0.2-µm focal planes throughout the entire cell (27 steps, 5 µm total) using a Plan Apo λ 1.4 NA 60x oil objective. For Supplemental Figure 2 A-T, cells were imaged in liquid medium under a coverslip, and images were acquired on the Andor W1 Spinning Disk Confocal at 32˚C using a Plan Apo λ 1.4 NA 60x oil objective. Sum projection images (non-deconvolved) were used for all quantitative analyses in Figure 4, Supplemental Figure 1D, and Supplemental Figure 2. For Figure 4, Supplemental Figure 1D, and Supplemental Figure 2, an ROI corresponding to the cytokinetic ring was drawn to measure integrated density. To measure background signal, the same ROI was moved to a place with no cells and this background signal was subtracted. For statistical analyses in Supplemental Figure 2, unpaired t-tests with Welch's correction were performed and p-values were determined by two-tailed distribution. For all statistical analyses, Graphpad Prism was used. For all statistical analyses, a single asterisk (*) denotes p-values < 0.05, two asterisks (**) indicate p-values < 0.01, three asterisks indicate p-value <0.001 and four asterisks (****) indicate p-value < 0.0001.

Acknowledgements

We thank members of the Moseley lab for comments on the manuscript. We thank the Biomolecular Targeting Core (BioMT) (P20-GM113132) and the Imaging Facility at Dartmouth for use of equipment. We also thank Jian-Qiu Wu, Juan Carlos Ribas, Dan McCollum, and Vladimir Sirotkin for sharing strains. This work was supported by grants from the American Cancer Society (RSG-15-140-01) and the National Institute of General Medical Sciences (R01GM099774) to J.B.M. K.L.S. was supported by a T-32 Training Grant (T32GM008704).

References

Almonacid, M., Moseley, J.B., Janvore, J., Mayeux, A., Fraisier, V., Nurse, P., and Paoletti, A. (2009). Spatial Control of Cytokinesis by Cdr2 Kinase and Mid1/Anillin Nuclear Export. Current Biology *19*, 961–966.

Almonacid, M., Celton-Morizur, S., Jakubowski, J.L., Dingli, F., Loew, D., Mayeux, A., Chen, J.-S., Gould, K.L., Clifford, D.M., and Paoletti, A. (2011). Temporal control of contractile ring assembly by Plo1 regulation of myosin II recruitment by Mid1/anillin. Curr. Biol. *21*, 473–479.

Arasada, R., and Pollard, T.D. (2014). Contractile Ring Stability in S. pombe Depends on F-BAR Protein Cdc15p and Bgs1p Transport from the Golgi Complex. Cell Reports *8*, 1533–1544.

Bähler, J., and Pringle, J.R. (1998). Pom1p, a fission yeast protein kinase that provides positional information for both polarized growth and cytokinesis. Genes Dev. *12*, 1356–1370.

Bähler, J., Steever, A.B., Wheatley, S., Wang, Y. l, Pringle, J.R., Gould, K.L., and McCollum, D. (1998a). Role of polo kinase and Mid1p in determining the site of cell division in fission yeast. J. Cell Biol. *143*, 1603–1616.

Bähler, J., Wu, J.Q., Longtine, M.S., Shah, N.G., McKenzie, A., Steever, A.B., Wach, A., Philippsen, P., and Pringle, J.R. (1998b). Heterologous modules for efficient and versatile PCR-based gene targeting in Schizosaccharomyces pombe. Yeast *14*, 943–951.

Burgess, A., Vigneron, S., Brioudes, E., Labbé, J.-C., Lorca, T., and Castro, A. (2010). Loss of human Greatwall results in G2 arrest and multiple mitotic defects due to deregulation of the cyclin B-Cdc2/PP2A balance. Proceedings of the National Academy of Sciences *107*, 12564–12569.

Celton-Morizur, S., Racine, V., Sibarita, J.-B., and Paoletti, A. (2006). Pom1 kinase links division plane position to cell polarity by regulating Mid1p cortical distribution. J. Cell. Sci. *119*, 4710–4718.

Chang, F., Woollard, A., and Nurse, P. (1996). Isolation and characterization of fission yeast mutants defective in the assembly and placement of the contractile actin ring. J. Cell. Sci. *109 (Pt 1)*, 131–142.

Chica, N., Rozalén, A.E., Pérez-Hidalgo, L., Rubio, A., Novak, B., and Moreno, S. (2016). Nutritional Control of Cell Size by the Greatwall-Endosulfine-PP2A·B55 Pathway. Current Biology *26*, 319–330.

Clifford, D.M., Wolfe, B.A., Roberts-Galbraith, R.H., McDonald, W.H., Yates, J.R., and Gould, K.L. (2008). The Clp1/Cdc14 phosphatase contributes to the robustness of cytokinesis by association with anillin-related Mid1. J. Cell Biol. *181*, 79–88.

Cundell, M.J., Bastos, R.N., Zhang, T., Holder, J., Gruneberg, U., Novak, B., and Barr, F.A. (2013). The BEG (PP2A-B55/ENSA/Greatwall) Pathway Ensures Cytokinesis follows Chromosome Separation. Molecular Cell *52*, 393–405.

Daga, R.R., and Chang, F. (2005). Dynamic positioning of the fission yeast cell division plane. Proceedings of the National Academy of Sciences *102*, 8228–8232.

Demeter, J., and Sazer, S. (1998). imp2, a new component of the actin ring in the fission yeast Schizosaccharomyces pombe. J. Cell Biol. *143*, 415–427.

Deng, L., Lee, M.E., Schutt, K.L., and Moseley, J.B. (2017). Phosphatases Generate Signal Specificity Downstream of Ssp1 Kinase in Fission Yeast. Mol. Cell. Biol. *37*.

G. Cortés, J.C., Pujol, N., Sato, M., Pinar, M., Ramos, M., Moreno, B., Osumi, M., Ribas, J.C., and Pérez, P. (2015). Cooperation between Paxillin-like Protein Pxl1 and Glucan Synthase Bgs1 Is Essential for Actomyosin Ring Stability and Septum Formation in Fission Yeast. PLOS Genetics *11*, e1005358.

Goyal, A., and Simanis, V. (2012). Characterization of *ypa1* and *ypa2* , the *Schizosaccharomyces pombe* Orthologs of the Peptidyl Proyl Isomerases That Activate PP2A, Reveals a Role for Ypa2p in the Regulation of Cytokinesis. Genetics *190*, 1235–1250.

Hanyu, Y., Imai, K.K., Kawasaki, Y., Nakamura, T., Nakaseko, Y., Nagao, K., Kokubu, A., Ebe, M., Fujisawa, A., Hayashi, T., et al. (2009). *Schizosaccharomyces pombe* cell division cycle under limited glucose requires Ssp1 kinase, the putative CaMKK, and Sds23, a PP2A-related phosphatase inhibitor. Genes to Cells *14*, 539–554.

Ishii, K., Kumada, K., Toda, T., and Yanagida, M. (1996). Requirement for PP1 phosphatase and 20S cyclosome/APC for the onset of anaphase is lessened by the dosage increase of a novel gene sds23+. EMBO J. *15*, 6629–6640.

Jang, Y.J., Won, M., Chung, K.S., Kim, D.U., Hoe, K.L., Park, C., and Yoo, H.S. (1997). A novel protein, Psp1, essential for cell cycle progression of Schizosaccharomyces pombe is phosphorylated by Cdc2-Cdc13 upon entry into G0-like stationary phase of cell growth. J. Biol. Chem. *272*, 19993–20002.

Jang, Y.-J., Won, M., and Yoo, H.-S. (2013). Phosphorylations of Sds23/Psp1/Moc1 by stress-activated kinase and cAMP-dependent kinase are essential for regulating cell viability in prolonged stationary phase: Sds23 phosphorylation and viability in stationary phase. Yeast n/a-n/a.

Jiang, W., and Hallberg, R.L. (2000). Isolation and characterization of par1(+) and par2(+): two Schizosaccharomyces pombe genes encoding B' subunits of protein phosphatase 2A. Genetics *154*, 1025–1038.

Jiang, W., and Hallberg, R.L. (2001). Correct regulation of the septation initiation network in Schizosaccharomyces pombe requires the activities of par1 and par2. Genetics *158*, 1413–1429.

Jochová, J., Rupes, I., and Streiblová, E. (1991). F-actin contractile rings in protoplasts of the yeast Schizosaccharomyces. Cell Biol. Int. Rep. *15*, 607–610.

Kinoshita, K., Nemoto, T., Nabeshima, K., Kondoh, H., Niwa, H., and Yanagida, M. (1996). The regulatory subunits of fission yeast protein phosphatase 2A (PP2A) affect cell morphogenesis, cell wall synthesis and cytokinesis. Genes Cells *1*, 29–45.

Lahoz, A., Alcaide-Gavilán, M., Daga, R.R., and Jimenez, J. (2010). Antagonistic roles of PP2A-Pab1 and Etd1 in the control of cytokinesis in fission yeast. Genetics *186*, 1261–1270.

Laplante, C., Huang, F., Tebbs, I.R., Bewersdorf, J., and Pollard, T.D. (2016). Molecular organization of cytokinesis nodes and contractile rings by super-resolution fluorescence microscopy of live fission yeast. Proceedings of the National Academy of Sciences *113*, E5876–E5885.

Le Goff, X., Buvelot, S., Salimova, E., Guerry, F., Schmidt, S., Cueille, N., Cano, E., and Simanis, V. (2001). The protein phosphatase 2A B'-regulatory subunit par1p is implicated in regulation of the S. pombe septation initiation network. FEBS Lett. *508*, 136–142.

Liu, J., Wang, H., McCollum, D., and Balasubramanian, M.K. (1999). Drc1p/Cps1p, a 1,3-beta-glucan synthase subunit, is essential for division septum assembly in Schizosaccharomyces pombe. Genetics *153*, 1193–1203.

Liu, J., Tang, X., Wang, H., Oliferenko, S., and Balasubramanian, M.K. (2002). The localization of the integral membrane protein Cps1p to the cell division site is dependent on the actomyosin ring and the septation-inducing network in Schizosaccharomyces pombe. Mol. Biol. Cell *13*, 989–1000.

Martin-Garcia, R., Coll, P.M., and Perez, P. (2014). F-BAR domain protein Rga7 collaborates with Cdc15 and Imp2 to ensure proper cytokinesis in fission yeast. Journal of Cell Science *127*, 4146–4158.

Martín-García, R., Arribas, V., Coll, P.M., Pinar, M., Viana, R.A., Rincón, S.A., Correa-Bordes, J., Ribas, J.C., and Pérez, P. (2018). Paxillin-Mediated Recruitment of Calcineurin to the Contractile Ring Is Required for the Correct Progression of Cytokinesis in Fission Yeast. Cell Reports *25*, 772-783.e4.

McDonald, N.A., Vander Kooi, C.W., Ohi, M.D., and Gould, K.L. (2015). Oligomerization but Not Membrane Bending Underlies the Function of Certain F-BAR Proteins in Cell Motility and Cytokinesis. Developmental Cell *35*, 725–736.

McDonald, N.A., Takizawa, Y., Feoktistova, A., Xu, P., Ohi, M.D., Vander Kooi, C.W., and Gould, K.L. (2016). The Tubulation Activity of a Fission Yeast F-BAR Protein Is Dispensable for Its Function in Cytokinesis. Cell Reports *14*, 534–546.

McDonald, N.A., Lind, A.L., Smith, S.E., Li, R., and Gould, K.L. (2017). Nanoscale architecture of the Schizosaccharomyces pombe contractile ring. ELife *6*.

Mishra, M., Karagiannis, J., Trautmann, S., Wang, H., McCollum, D., and Balasubramanian, M.K. (2004). The Clp1p/Flp1p phosphatase ensures completion of cytokinesis in response to

minor perturbation of the cell division machinery in Schizosaccharomyces pombe. J. Cell. Sci. *117*, 3897–3910.

Mochida, S., Maslen, S.L., Skehel, M., and Hunt, T. (2010). Greatwall phosphorylates an inhibitor of protein phosphatase 2A that is essential for mitosis. Science *330*, 1670–1673.

Moreno, S., Klar, A., and Nurse, P. (1991). Molecular genetic analysis of fission yeast Schizosaccharomyces pombe. Meth. Enzymol. *194*, 795–823.

Padte, N.N., Martin, S.G., Howard, M., and Chang, F. (2006). The cell-end factor pom1p inhibits mid1p in specification of the cell division plane in fission yeast. Curr. Biol. *16*, 2480–2487.

Pelham, R.J., and Chang, F. (2002). Actin dynamics in the contractile ring during cytokinesis in fission yeast. Nature *419*, 82–86.

Piekny, A.J., and Glotzer, M. (2008). Anillin Is a Scaffold Protein That Links RhoA, Actin, and Myosin during Cytokinesis. Current Biology *18*, 30–36.

Pollard, T.D., and Wu, J.-Q. (2010). Understanding cytokinesis: lessons from fission yeast. Nat. Rev. Mol. Cell Biol. *11*, 149–155.

Proctor, S.A., Minc, N., Boudaoud, A., and Chang, F. (2012). Contributions of turgor pressure, the contractile ring, and septum assembly to forces in cytokinesis in fission yeast. Curr. Biol. *22*, 1601–1608.

Roberts-Galbraith, R.H., Chen, J.-S., Wang, J., and Gould, K.L. (2009). The SH3 domains of two PCH family members cooperate in assembly of the *Schizosaccharomyces pombe* contractile ring. The Journal of Cell Biology *184*, 113–127.

Saitoh, S., Mori, A., Uehara, L., Masuda, F., Soejima, S., and Yanagida, M. (2015). Mechanisms of expression and translocation of major fission yeast glucose transporters regulated by CaMKK/phosphatases, nuclear shuttling, and TOR. Mol. Biol. Cell *26*, 373–386.

Schneider, C.A., Rasband, W.S., and Eliceiri, K.W. (2012). NIH Image to ImageJ: 25 years of image analysis. Nat. Methods *9*, 671–675.

Sethi, K., Palani, S., Cortés, J.C.G., Sato, M., Sevugan, M., Ramos, M., Vijaykumar, S., Osumi, M., Naqvi, N.I., Ribas, J.C., et al. (2016). A New Membrane Protein Sbg1 Links the Contractile Ring Apparatus and Septum Synthesis Machinery in Fission Yeast. PLOS Genetics *12*, e1006383.

Sipiczki, M., and Bozsik, A. (2000). The use of morphomutants to investigate septum formation and cell separation in Schizosaccharomyces pombe. Arch. Microbiol. *174*, 386–392.

Snider, C.E., Willet, A.H., Chen, J.-S., Arpağ, G., Zanic, M., and Gould, K.L. (2017). Phosphoinositide-mediated ring anchoring resists perpendicular forces to promote medial cytokinesis. The Journal of Cell Biology *216*, 3041–3050.

Snider, C.E., Willet, A.H., Brown, H.T., and Gould, K.L. (2018). Analysis of the contribution of phosphoinositides to medial septation in fission yeast highlights the importance of PI(4,5)P_2 for medial contractile ring anchoring. Molecular Biology of the Cell *29*, 2148–2155.

Sohrmann, M., Fankhauser, C., Brodbeck, C., and Simanis, V. (1996). The dmf1/mid1 gene is essential for correct positioning of the division septum in fission yeast. Genes & Development *10*, 2707–2719.

Trautmann, S., Wolfe, B.A., Jorgensen, P., Tyers, M., Gould, K.L., and McCollum, D. (2001). Fission yeast Clp1p phosphatase regulates G2/M transition and coordination of cytokinesis with cell cycle progression. Curr. Biol. *11*, 931–940.

Wu, J.-Q., Kuhn, J.R., Kovar, D.R., and Pollard, T.D. (2003). Spatial and temporal pathway for assembly and constriction of the contractile ring in fission yeast cytokinesis. Dev. Cell *5*, 723–734.

Wu, J.-Q., Sirotkin, V., Kovar, D.R., Lord, M., Beltzner, C.C., Kuhn, J.R., and Pollard, T.D. (2006). Assembly of the cytokinetic contractile ring from a broad band of nodes in fission yeast. The Journal of Cell Biology *174*, 391–402.

Yakura, M., Ishikura, Y., Adachi, Y., and Kawamukai, M. (2006). Involvement of Moc1 in Sexual Development and Survival of *Schizosaccharomyces pombe*. Bioscience, Biotechnology, and Biochemistry *70*, 1740–1749.

Figure Legends

Figure 1. *sds23*Δ cells divide asymmetrically. (A) Representative images of cells of the indicated strains with cell wall stain. Inset is cell length ± standard deviation. Scale bar 5 µm. (B) Schematic depicting calculation of Cell Half Ratio. (C) Cell Half Ratios of the indicated strains as a measure of division asymmetry. ** indicates p-value < 0.01, **** indicates p-value < 0.0001.

Figure 2. Defects in nuclear positioning and ring assembly in *sds23*Δ cells. (A) Cell Half Ratio at time of ring assembly for the indicated strains. **** indicates p-value < 0.0001. (B) Duration of CAR assembly in wild type versus *sds23*Δ cells. (C) Montages displaying two representative cells of the indicated strains expressing Cut11-mCherry. Cut11-mCherry fluorescence signal has been overlaid onto DIC images to visualize the cell tips. Scale bar 8 µm, images acquired every 3 minutes. (D) Quantification of nuclear movement as a function of time for the indicated strains. **** indicates p-value < 0.0001. (E) Quantification of Mid1-mNeonGreen whole cell fluorescence in wild type, *sds23Δ,* and *cdc25-dd* cells. **** indicates p-value < 0.0001. (F) DIC and middle focal plane inverted fluorescence images of two representative wild type, *sds23Δ,* and *cdc25-dd* cells expressing Mid1-mNeonGreen. Scale bar 8 µm.

Figure 3. CAR sliding in *sds23*Δ cells. (A) Timelapse montages displaying a representative wild type, *sds23*Δ*,* and *cdc25-degron-DAmP* cell expressing Rlc1-mNeonGreen and Sad1-mEGFP. The first image of each montage is the time of SPB splitting. The pink dotted line indicates initial ring position for all montages. Images are inverted fluorescence of sum projections. Scale bar 8 µm. (B) Top: Schematic depicting ring displacement measurement. Bottom: Quantification of cytokinetic ring displacement. **** indicates p-value < 0.0001. (C) Duration of CAR maturation in wild type versus *sds23*Δ cells. **** indicates p-value < 0.0001. (D) DIC image of *sds23Δ efr3Δ*. Red asterisks indicate dead cells.

Figure 4. Delayed recruitment of CAR anchors in *sds23*Δ cells. (A) Timelapse images of GFP-Bgs1 recruitment in wild type versus *sds23*Δ cells. Images are inverted fluorescence of sum projections. Time "0" indicates SPB splitting as determined by Sad1 signal. Note, a 561 nm laser was used to image Sad1-mCherry, but only the signal from the 488 nm laser is displayed. Scale bar 8 µm. (B) Quantification of GFP-Bgs1 recruitment during cytokinesis in wild type versus *sds23*Δ cells. (C) Timelapse images for Imp2-mEGFP recruitment, as in panel A. (D) Quantification of Imp2-mEGFP recruitment during cytokinesis in wild type versus *sds23*Δ cells. (E) Timelapse images for Rga7-mEGFP recruitment, as in panel A. (F) Quantification of Rga7-mEGFP recruitment during cytokinesis in wild type versus *sds23*Δ cells.

Figure 5. Genetic interactions between Sds23 and Ppk18-Igo1. (A) Schematic depicting Igo1 and Sds23 interactions with Protein Phosphatase 2A (PP2A). Phosphorylation of Igo1 by Ppk18 promotes interaction with PP2A (Hanyu *et al.*, 2009; Chica *et al.*, 2016). (B) Representative images of cells of the indicated strains with cell wall stain. Scale bar 8 µm. (C) Quantification of bent cell shape phenotype for the indicated strains. (D) Cell Half Ratios of the indicated strains.

Supplemental Figure 1. Distribution of nodes and myosin recruitment are unaffected in *sds23*Δ. (A) Inverted fluorescence images of Pom1-mEGFP in wild type and *sds23*Δ cells. Scale bar 5 µm. (B) Top: Inverted max projection images of *cdc25-degron-DAmP* and *sds23*Δ cells expressing Cdr2-mEGFP. Scale bar 8 µm. Bottom: Full-Width Half Maximum (FWHM) of Cdr2-mEGFP signal comparing spread of nodes in *cdc25-degron-DAmP* and *sds23*Δ cells. (C) Time lapse images of wild type and *sds23*Δ cells expressing Rlc1-mNeonGreen and Sad1-mEGFP. Images are inverted fluorescence of sum projections. Scale bar 8 µm. (D) Quantification of Rlc1-mNeonGreen over time for wild type and *sds23*Δ.

Supplemental Figure 2. Screen for localization defects for putative CAR anchor proteins. (A-T) Quantification of the indicated CAR proteins in wild type and *sds23*Δ cells. * indicates p-value < 0.05, ** indicates p-value < 0.01, *** indicates p-value < 0.001, and **** indicates p-value < 0.0001.

Supplemental Figure 3. Elongating *igo1*Δ cells does not cause cytokinesis defects. (A) Representative images of cells of the indicated strains with cell wall stain. Scale bar 5 µm. (B) Cell Half Ratios of the indicated strains as a measure of division asymmetry.

Supplemental Table 1. Strains used in this study.

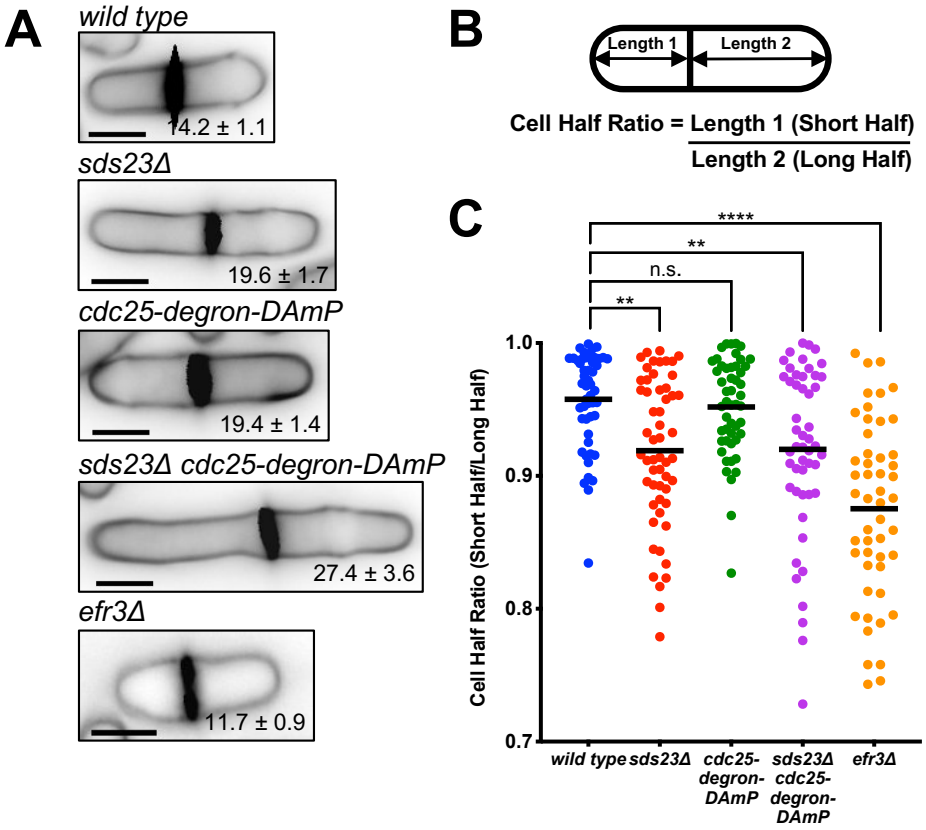
A
wild type
14.2 ± 1.1
sds23Δ
19.6 ± 1.7
cdc25-degron-DAmP
19.4 ± 1.4
sds23Δ cdc25-degron-DAmP
27.4 ± 3.6
efr3Δ
11.7 ± 0.9
B
Length 1
Length 2
Cell Half Ratio = Length 1 (Short Half) / Length 2 (Long Half)
C
****
**
n.s.
**
Cell Half Ratio (Short Half/Long Half)
1.0
0.9
0.8
0.7
wild type
sds23Δ
cdc25-degron-DAmP
sds23Δ cdc25-degron-DAmP
efr3Δ

Figure 1

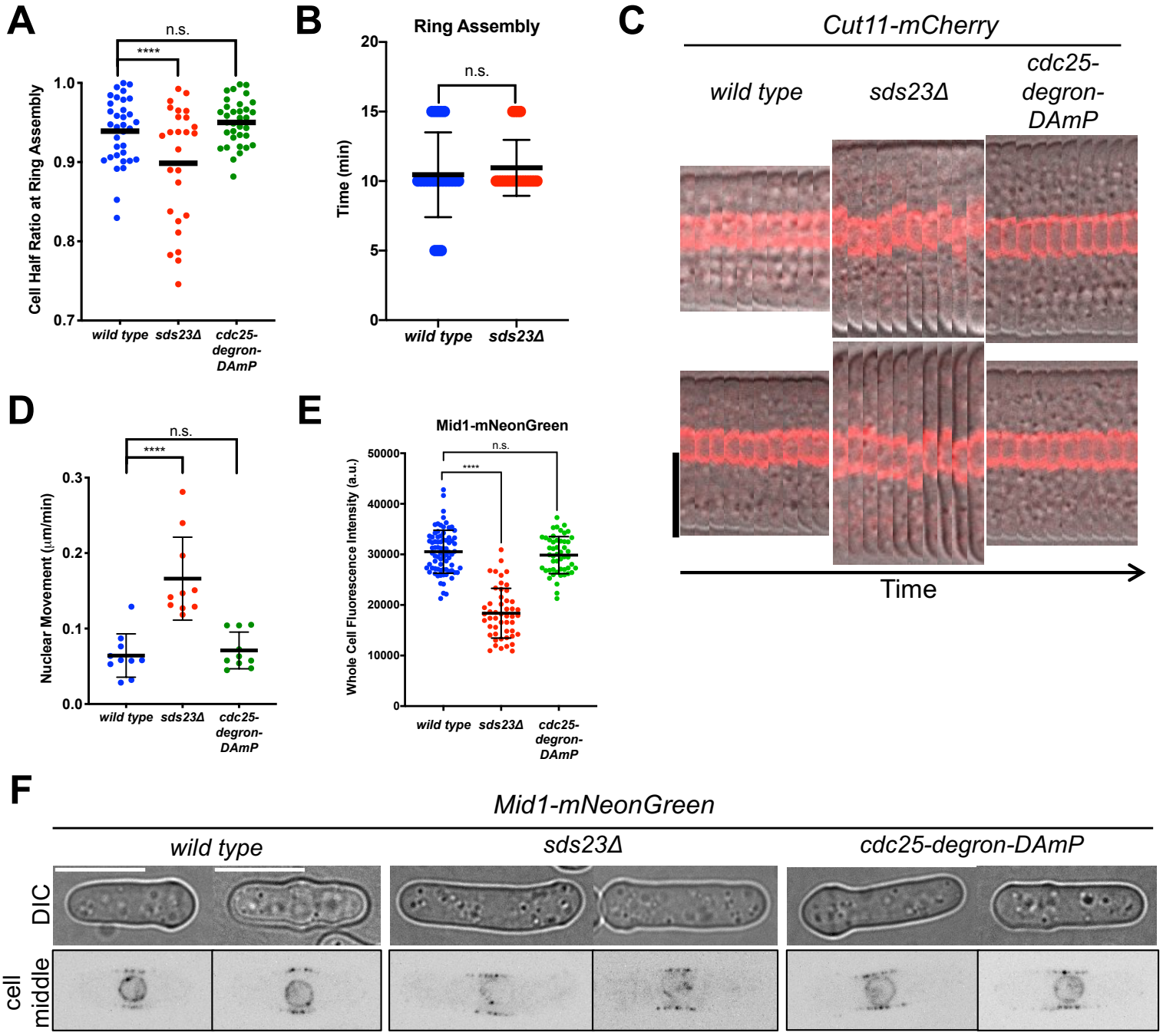
A
n.s.
****
Cell Half Ratio at Ring Assembly
1.0
0.9
0.8
0.7
wild type
sds23Δ
cdc25-degron-DAmP
B
Ring Assembly
n.s.
Time (min)
20
15
10
5
0
wild type
sds23Δ
C
Cut11-mCherry
wild type
sds23Δ
cdc25-degron-DAmP
Time
D
n.s.
****
Nuclear Movement (μm/min)
0.3
0.2
0.1
0.0
wild type
sds23Δ
cdc25-degron-DAmP
E
Mid1-mNeonGreen
n.s.
****
Whole Cell Fluorescence Intensity (a.u.)
50000
40000
30000
20000
10000
0
wild type
sds23Δ
cdc25-degron-DAmP
F
Mid1-mNeonGreen
wild type
sds23Δ
cdc25-degron-DAmP
DIC
cell middle

Figure 2

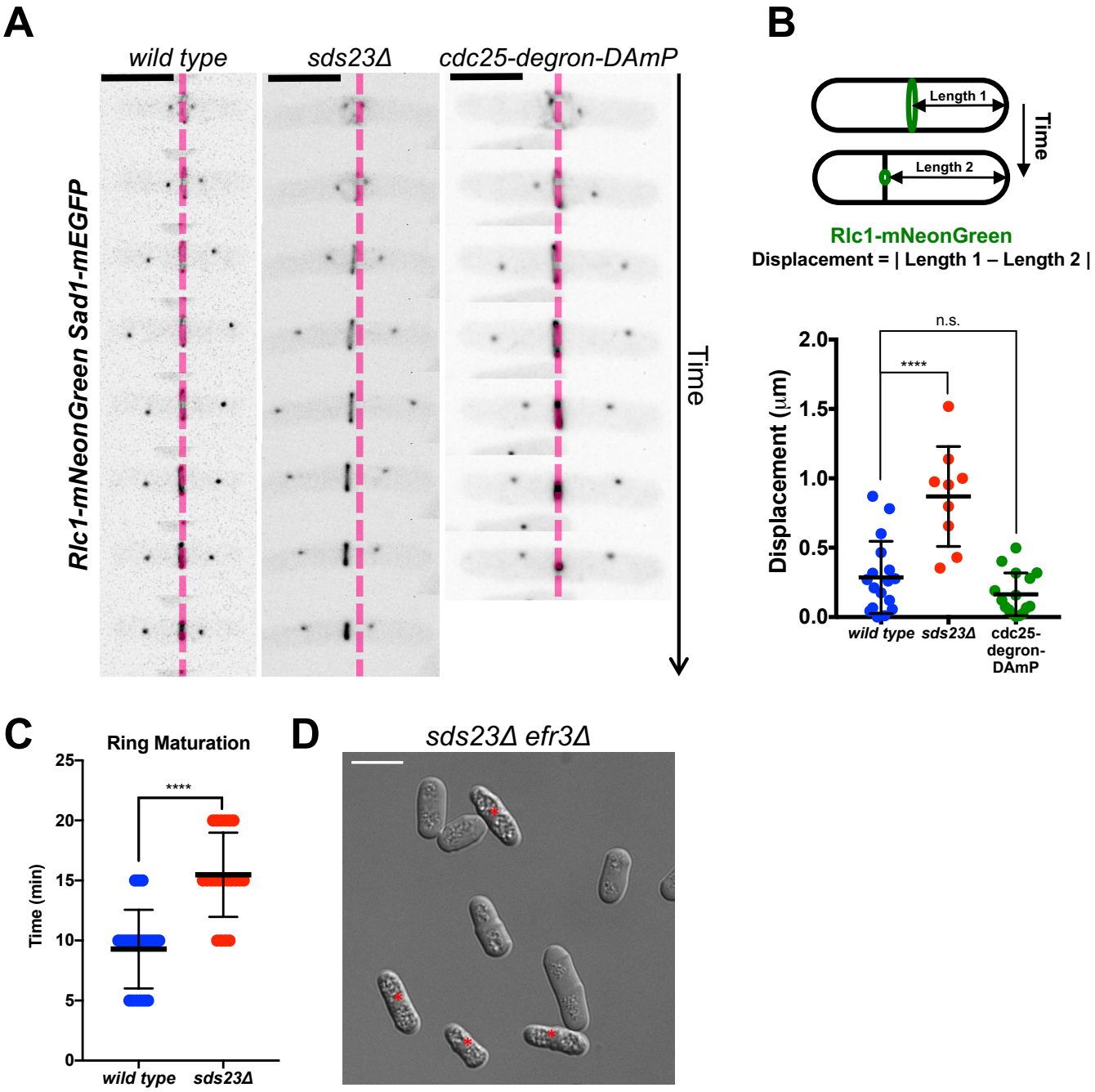
A
wild type
sds23Δ
cdc25-degron-DAmP
Rlc1-mNeonGreen Sad1-mEGFP
Time
B
Length 1
Length 2
Time
Rlc1-mNeonGreen
Displacement = | Length 1 – Length 2 |
n.s.
****
Displacement (μm)
2.0
1.5
1.0
0.5
0.0
wild type
sds23Δ
cdc25-degron-DAmP
C
Ring Maturation
****
Time (min)
25
20
15
10
5
0
wild type
sds23Δ
D
sds23Δ efr3Δ

Figure 3

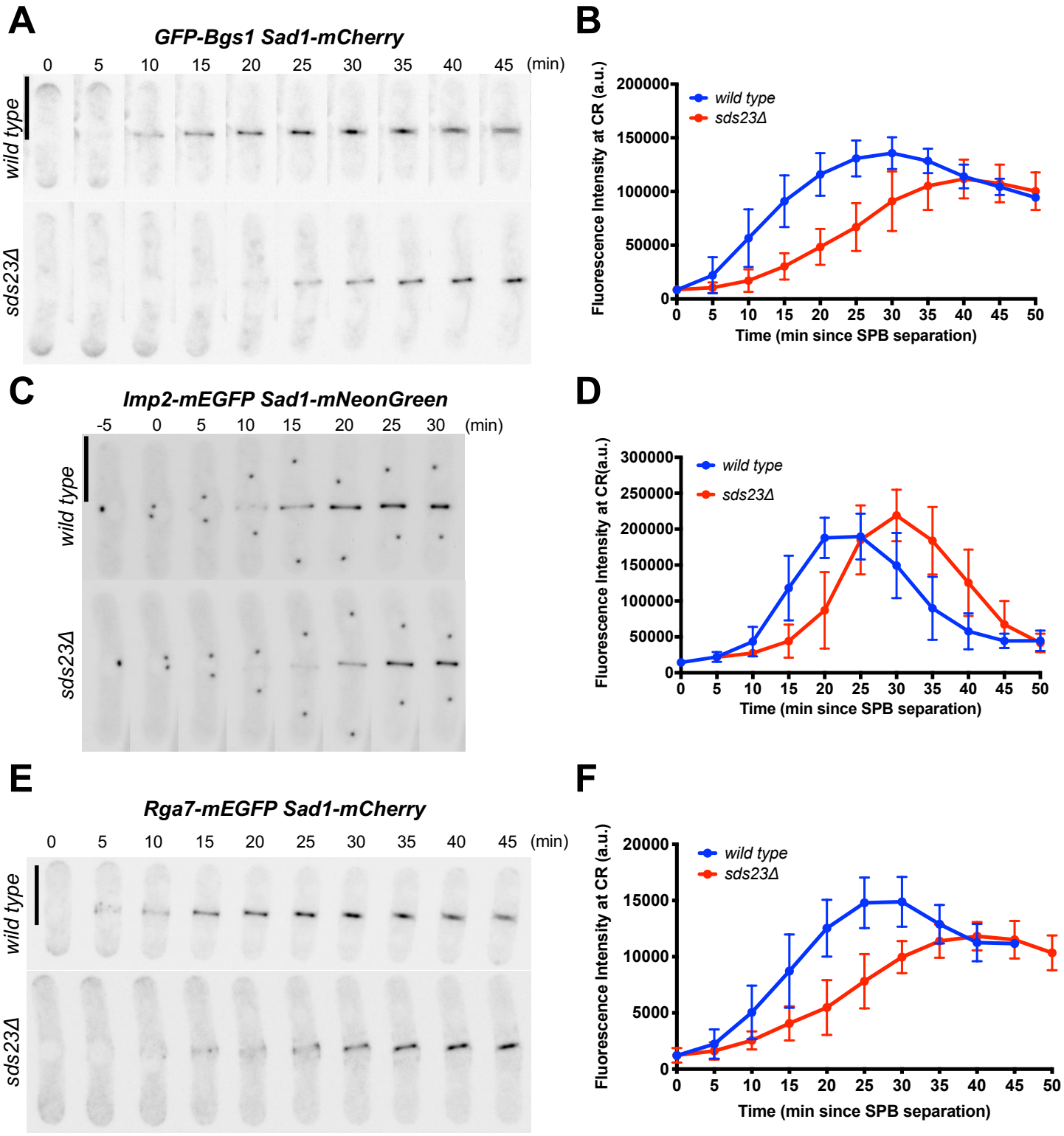
A
GFP-Bgs1 Sad1-mCherry
0 5 10 15 20 25 30 35 40 45 (min)
wild type
sds23Δ
B
Fluorescence Intensity at CR (a.u.)
200000
150000
100000
50000
0
wild type
sds23Δ
0 5 10 15 20 25 30 35 40 45 50
Time (min since SPB separation)
C
Imp2-mEGFP Sad1-mNeonGreen
-5 0 5 10 15 20 25 30 (min)
wild type
sds23Δ
D
Fluorescence Intensity at CR(a.u.)
300000
250000
200000
150000
100000
50000
0
wild type
sds23Δ
0 5 10 15 20 25 30 35 40 45 50
Time (min since SPB separation)
E
Rga7-mEGFP Sad1-mCherry
0 5 10 15 20 25 30 35 40 45 (min)
wild type
sds23Δ
F
Fluorescence Intensity at CR (a.u.)
20000
15000
10000
5000
0
wild type
sds23Δ
0 5 10 15 20 25 30 35 40 45 50
Time (min since SPB separation)

Figure 4

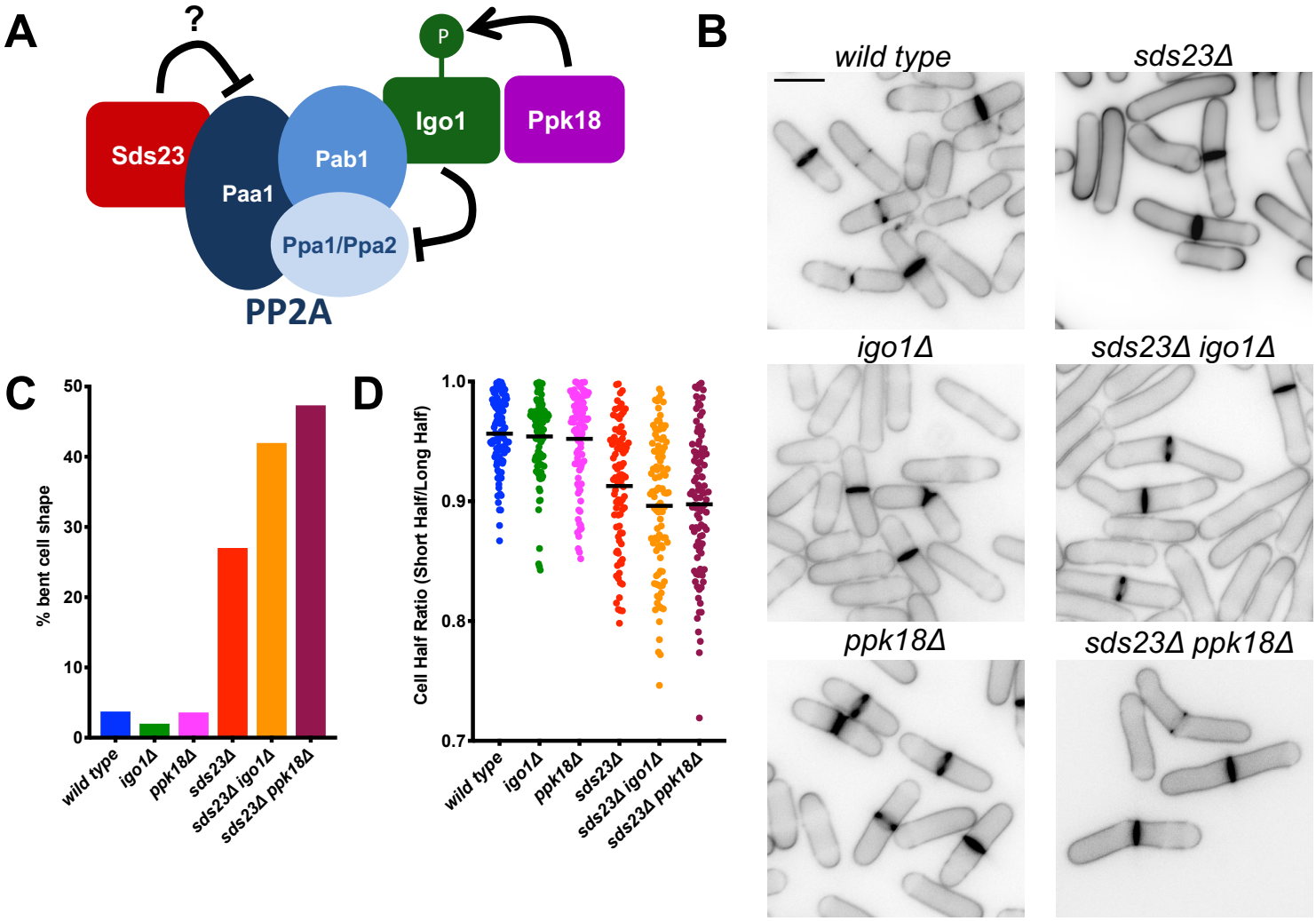
A
?
P
Sds23
Paa1
Pab1
Igo1
Ppk18
Ppa1/Ppa2
PP2A
B
wild type
sds23Δ
igo1Δ
sds23Δ igo1Δ
ppk18Δ
sds23Δ ppk18Δ
C
% bent cell shape
50
40
30
20
10
0
wild type
igo1Δ
ppk18Δ
sds23Δ
sds23Δ igo1Δ
sds23Δ ppk18Δ
D
Cell Half Ratio (Short Half/Long Half)
1.0
0.9
0.8
0.7
wild type
igo1Δ
ppk18Δ
sds23Δ
sds23Δ igo1Δ
sds23Δ ppk18Δ

Figure 5

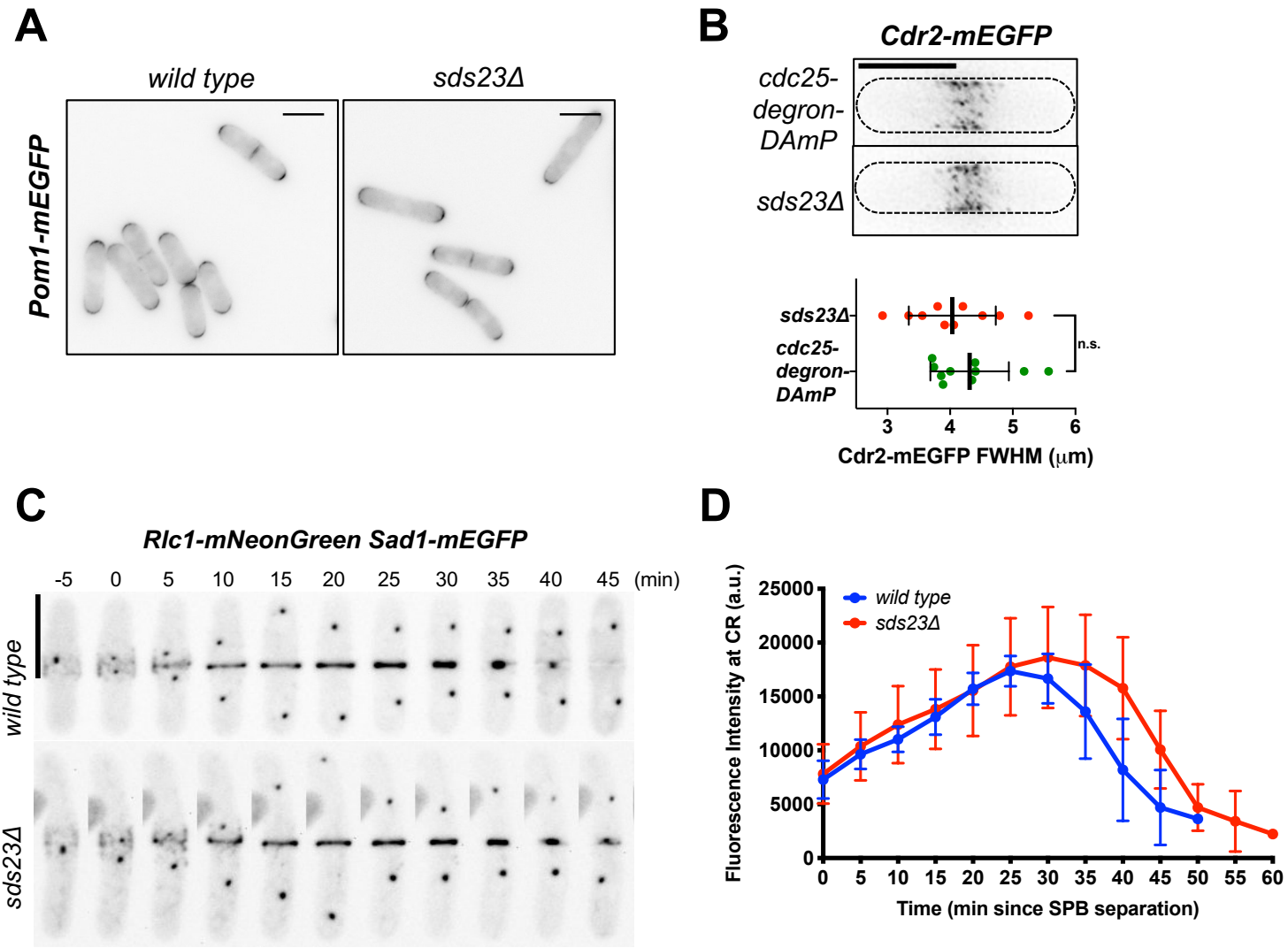
A
wild type
sds23Δ
Pom1-mEGFP
B
Cdr2-mEGFP
cdc25-degron-DAmP
sds23Δ
sds23Δ
cdc25-degron-DAmP
n.s.
3
4
5
6
Cdr2-mEGFP FWHM (μm)
C
Rlc1-mNeonGreen Sad1-mEGFP
-5
0
5
10
15
20
25
30
35
40
45
(min)
wild type
sds23Δ
D
wild type
sds23Δ
Fluorescence Intensity at CR (a.u.)
25000
20000
15000
10000
5000
0
0
5
10
15
20
25
30
35
40
45
50
55
60
Time (min since SPB separation)

Figure S1

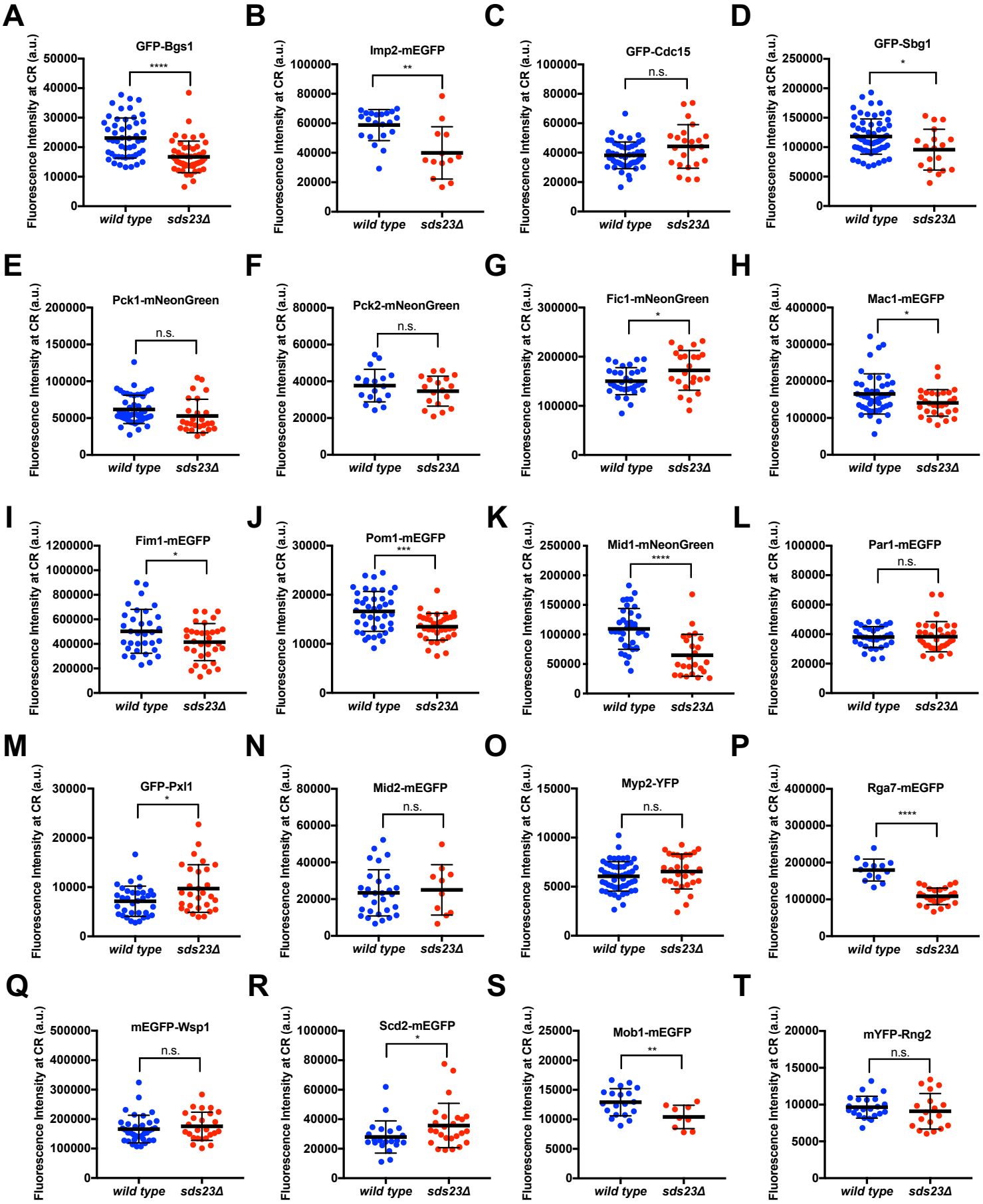
A
GFP-Bgs1
****
B
Imp2-mEGFP
**
C
GFP-Cdc15
n.s.
D
GFP-Sbg1
*
E
Pck1-mNeonGreen
n.s.
F
Pck2-mNeonGreen
n.s.
G
Fic1-mNeonGreen
*
H
Mac1-mEGFP
*
I
Fim1-mEGFP
*
J
Pom1-mEGFP
***
K
Mid1-mNeonGreen
****
L
Par1-mEGFP
n.s.
M
GFP-Pxl1
*
N
Mid2-mEGFP
n.s.
O
Myp2-YFP
n.s.
P
Rga7-mEGFP
****
Q
mEGFP-Wsp1
n.s.
R
Scd2-mEGFP
*
S
Mob1-mEGFP
**
T
mYFP-Rng2
n.s.
Fluorescence Intensity at CR (a.u.)
wild type
sds23Δ

Figure S2

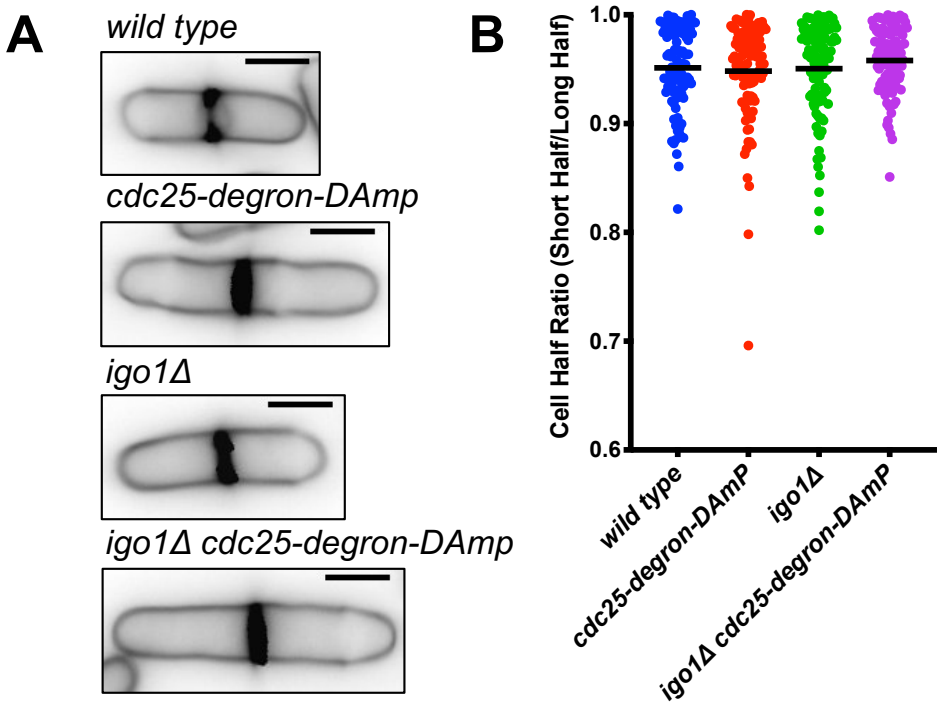
A
wild type
cdc25-degron-DAmp
igo1Δ
igo1Δ cdc25-degron-DAmp
B
Cell Half Ratio (Short Half/Long Half)
1.0
0.9
0.8
0.7
0.6
wild type
cdc25-degron-DAmP
igo1Δ
igo1Δ cdc25-degron-DAmP

Figure S3